The Astronomical Journal, 166:179 (8pp), 2023 October https://doi.org/10.3847/1538-3881/acf56f

Three-dimensional MHD Simulations of the Magnetic Pileup at Mars

M. Wang[1,2], Z. J. Guan[1], L. Xie[2,3], J. Y. Lu[1], X. Xu[4,5], Y. Wei[6,7], Z. Zhou[4,5], L. Chai[6,7], J. Wang[8], Q. Chang[4,5], H. X. Zhang[1], B. H. Qu[1], H. Y. Sui[1], J. Q. Zhang[1], F. H. Qiao[2,3], and L. Li[2,3]
[1] Institute of Space Weather, Nanjing University of Information Science and Technology, Nanjing, People's Republic of China; jylu@nuist.edu.cn
[2] State Key Laboratory of Space Weather, National Space Science Center, Chinese Academy of Sciences, Beijing, People's Republic of China; xielianghai@nssc.ac.cn
[3] Joint Research and Development Center of Chinese Science Academy and Shen county, Shandong, People's Republic of China
[4] State Key Laboratory of Lunar and Planetary Sciences, Macau University of Science and Technology, Macau, People's Republic of China
[5] CNSA Macau Center for Space Exploration and Science, Macau, People's Republic of China
[6] Key Laboratory of Earth and Planetary Physics, Institute of Geology and Geophysics, Chinese Academy of Sciences, Beijing, People's Republic of China
[7] College of Earth and Planetary Sciences, University of Chinese Academy of Sciences, Beijing, People's Republic of China
[8] Planetary Environmental and Astrobiological Research Laboratory (PEARL), School of Atmospheric Sciences, Sun Yatsen University, Zhuhai, People's Republic of China; jylu@nuist.edu.cn
Received 2023 May 12; revised 2023 August 21; accepted 2023 August 29; published 2023 September 29

Abstract

In this study, we introduced a quantitative parameter, the magnetic field strength difference, to denote the intensity of the magnetic pileup effect at Mars. Using a three-dimensional multispecies MHD model, the effects of the interplanetary magnetic field (IMF) and the solar wind dynamic pressure (P_d) constituted with different densities and velocities on the magnetic pileup were examined. Our results show that: (1) the magnetic pileup at Mars mainly occurs at the dayside region and its magnitude is generally decreasing with increasing solar zenith angle. The magnetic pileup is generally weak in the intense crustal field region, while it is strong in the weak crustal field region. (2) The perpendicular IMF components, B_Y and B_Z, dominate the magnetic pileup, while the radial IMF component, B_X, has little effect. In the intense crustal field region, when the IMF and crustal field are primarily in the same direction, the magnetic field is piled up and the pileup magnitude is generally strong. While the directions of the crustal field and IMF are opposite, the occurrence of magnetic reconnection can weaken the local magnetic pileup. (3) Under the same P_d, a higher solar wind velocity results in a higher intensity and a larger region of the magnetic pileup. When P_d increases, the magnitude of the magnetic pileup is enhanced, but the pileup region shrinks. In addition, for an increasing P_d, at the center of the induced magnetotail, the asymmetric current sheet can lead to similar asymmetries of the pileup.

Unified Astronomy Thesaurus concepts: Interplanetary magnetic fields (824); Planetary magnetospheres (997); Mars (1007); Solar wind (1534)

1. Introduction

Mars represents an unmagnetized body with an atmosphere (e.g., Acuna et al. 1999). When solar wind interacts with Mars, the interplanetary magnetic field (IMF) can pile up around the unmagnetized obstacle and form an induced magnetosphere (e.g., Nagy et al. 2004). The interaction can start from thousands of kilometers away from the planet, where the neutral exospheric particles are ionized by both photoionization and charge-exchange ionization, and accelerated by the solar wind convection electric field ($\boldsymbol{E}_{\rm SW} = -\boldsymbol{V}_{\rm SW} \times \boldsymbol{B}_{\rm IMF}$; e.g., Szegö et al. 2000). Then, these newborn ions are picked up and moved with the solar wind, leading to a mass loading and a decrease in the solar wind velocity (e.g., Matsunaga et al. 2017). The magnetic field can slightly pile up due to the decrease, which brings in an increase in the magnetic field strength (e.g., Bertucci et al. 2003). In addition, the Martian ionopause provides a diamagnetic current that is sometimes strong enough to prevent the penetration of the solar wind magnetic field into the ionosphere (e.g., Dubinin et al. 2019). As a result, the magnetic field can significantly pile up around the ionosphere, resulting in the so-called magnetic pileup region. Moreover, both the mass loading and the diamagnetic current are more remarkable near the subsolar region (e.g., Fang et al. 2018). Consequently, the IMF can drape around the ionosphere, leading to the formation two lobes in the magnetotail region (e.g., Crider et al. 2004; Rong et al. 2016). Therefore, magnetic pileup is essential for the formation of the induced magnetosphere of Mars.

Along with the magnetic pileup on the dayside, both the magnetic field strength and the magnetic pressure are enhanced. The plasmas near the plasma depletion region (the inner part of the Martian magnetosheath where the magnetic fields are enhanced and the plasma densities are partially depleted) can be squeezed out along the piled-up magnetic field, leading to a decrease in plasma β, plasma density, and ion temperature, especially for the hotter plasmas (e.g., Bertucci et al. 2003; Øieroset et al. 2004; Wang et al. 2020a). On the other hand, the piled-up magnetic field may reconnect with the local crustal field or the other draped fields (e.g., Halekas et al. 2009), which would lead to a different magnetic field morphology at Mars that can further affect the large-scale structures of the Martian induced magnetosphere (such as the magnetic pileup boundary (MPB) and the bow shock; e.g., Vignes et al. 2000; Wang et al. 2020b, 2021, 2022), the planetary pickup ion acceleration (e.g., Fang et al. 2008; Halekas et al. 2017), the ion escape (e.g., Wei et al. 2012; Harada et al. 2018; Fan et al. 2019; Xu et al. 2022b), the plasma sheet orientation (e.g., DiBraccio et al.

2018), the global looping magnetic field (e.g., Chai et al. 2019), and the current systems at Mars (e.g., Baumjohann et al. 2010; Ramstad et al. 2020). Hence, the magnetic pileup plays a vital role in studying the plasma environment and the atmospheric ion loss of Mars.

However, the details of the magnetic pileup at Mars have not been thoroughly investigated. First, it was reported that the IMF is roughly piled up at the subsolar region between the bow shock and the ionopause at an altitude of 600–1000 km (Vignes et al. 2000; Vennerstrom et al. 2003). Recently, using a time-dependent global magnetohydrodynamic model, Fang et al. (2018) studied the magnetic field draping pattern in the Martian magnetosheath and indicated that the magnetic field clock angle departure in the magnetosheath increases with decreasing altitude and increasing solar zenith angle (SZA), which can affect the magnetic pileup conditions there. However, the details of the magnetic pileup region, including its distribution and correlation with SZA, are less investigated. Second, as the magnetic pileup is significantly related to the ion pickup and mass loading processes driven by the solar wind convection electric field, the magnetic pileup condition should vary with the upstream solar wind parameters. However, although the IMF effects on the properties of the Martian magnetic field have been studied (e.g., Brain et al. 2006; Luhmann et al. 2015), the influences of the upstream solar wind on the magnetic pileup are rarely reported. In addition, the intensity of the magnetic pileup has not been clearly defined in the current works of literature.

In this paper, the magnetic pileup of Mars will be quantitatively studied with a three-dimensional multispecies MHD model. Moreover, the effects of different IMF conditions, solar wind densities, and velocities on the magnetic pileup will be discussed.

2. Simulation and Method

In this work, the three-dimensional multispecies MHD model initially developed by Ma et al. (2004) was employed to study the interaction between the solar wind and the Martian induced magnetosphere. This model is implemented within the Block Adaptive-Tree Solar wind Roe-type Upwind Scheme in the Space Weather Modeling Framework (Tóth et al. 2012). Recently, we have utilized this model to investigate the Martian bow shock (Wang et al. 2020b) and the MPB (Wang et al. 2021, 2022), the effectiveness and reliability of this model have also been verified by plenty of studies (Fang et al. 2008, 2010a, 2010b, 2018; Ma et al. 2014a, 2014b). The details of the model information are given by Ma et al. (2004). The Martian crustal field is described using the 60 order spherical harmonic model developed by Arkani-Hamed (2001). In this work, the model input parameters were set as follows: first, all the simulations were fixed with the strongest Martian crustal magnetic field located on the dayside (180°W 0°N) under the solar maximum conditions, which are identical to Case 1 of Ma et al. (2004). Next, the Y and Z components of the solar wind velocity, V_Y and V_Z, were chosen to be 0, and the upstream solar wind ion temperature $T_i = 5 \times 10^4$ and electron temperature $T_e = 3 \times 10^5$ K. Then, the different solar wind conditions constituted by the velocity V_X, the number density (n), and the components of IMF (B_X, B_Y, B_Z) in the Mars-centered solar orbital (MSO) coordinate system were simulated to study the magnetic pileup conditions at Mars.

As we mentioned before, when the magnetic pileup occurs on Mars, some properties of the plasma should be changed in the pileup region, including an increase in magnetic field strength (e.g., Bertucci et al. 2003; Øieroset et al. 2004; Wang et al. 2020a). Actually, the enhancement of magnetic field strength in the pileup region consists of two parts: the compression of the Martian crustal magnetic field and the pileup of IMF. On the one hand, the solar wind interaction with Mars can push its crustal field close to the Martian surface, resulting in the increase of magnetic field strength in the crustal field region. On the other hand, under typical upstream conditions, the pileup of IMF due to the solar wind mass loading process can also add to the magnetic field's magnitude for the majority of regions. The compression of the crustal field is always present, while the IMF pileup conditions change with the upstream solar wind parameters. Hence, in this work, we eliminated the compression result of the Martian crustal magnetic field and employed the change of the magnetic field strength due to the IMF pileup to represent the magnetic pileup result. It is worth mentioning that the enhancement of magnetic field strength does not always happen in the typical pileup regions. Due to the compression of the solar wind, at the place that was dominated by the crustal field and is now occupied by the solar wind, the magnetic field strength should be decreased. In addition, the topology of the Martian crustal field and the magnetic reconnection may also play a role, which will be discussed in detail next.

Figure 1 shows the difference in magnetic field intensity, dB_t, at Mars under normal solar wind conditions. Panels (a) and (d) display the difference values of B_t between the steady state under the IMF condition of zero intensity ($Bt_{\mathrm{IMF=0}}$) and the initial time state of the pure Martian crustal field (Bt_{C}), which represent the difference values of B_t caused by the compression of the Martian crustal field. Panels (b) and (e) show the difference values of B_t between the steady state under the Parker-spiral IMF condition ($Bt_{\mathrm{ParkerIMF}}$) and the initial Martian crustal field state (Bt_{C}), which stand for the total difference values of B_t due to both of the crustal field compression and the IMF pileup under the Parker-spiral IMF case. Panels (c) and (f) display the difference values of B_t under the steady state between the Parker-spiral IMF condition and IMF = 0, which represent the dB_t caused by the pileup of the Parker-spiral IMF. Hence, in this work, the dB_t between the corresponding IMF condition and IMF = 0 under the steady state is employed to represent the magnetic pileup result. It is worth mentioning that, the zero IMF intensity case (IMF = 0) does not mean that the IMF intensity is precisely equal to zero. Actually, this case was carried out with the very tiny values of the IMF components, such as 0.01 nT. The Parker-spiral IMF condition was set with $B_X = -1.6776$ nT, $B_Y = 2.4871$ nT, and $B_Z = 0$ nT (Ma et al. 2004).

Figure 1 displays that the magnetic pileup at Mars mainly occurs at the dayside region ($X > 0$ R_M) for both X–Y and X–Z planes. The enhancement of magnetic field strength because of the compression of the Martian crustal magnetic field is relatively weak (the difference values of $B_t \approx 10$ nT in panels (a) and (d)), while it appears stronger for the pileup of the Parker-spiral IMF case (dB_t can reach 30 nT in panels (c) and (f)). At the dayside region of the Parker-spiral IMF pileup (panels (c) and (f)), the magnetic pileup intensity generally decreases with increasing SZA. Moreover, some asymmetries also appear in that the pileup at the duskside hemisphere

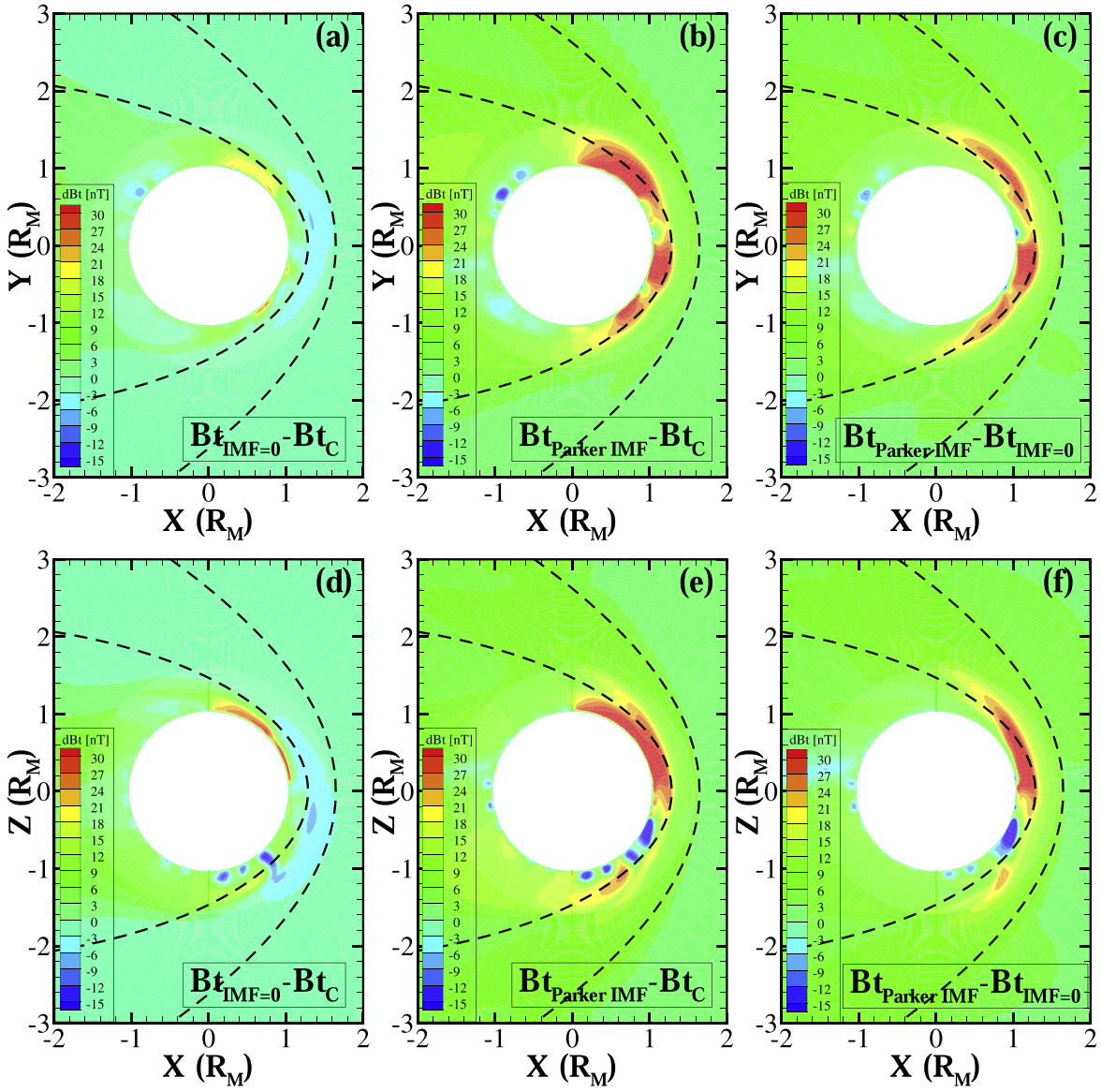

Figure 1. The difference in magnetic field intensity, dB_t, on the X–Y (upper panels) and X–Z (bottom panels) planes in the MSO coordinate system for $P_d = 1.06$ nPa ($n = 4.0$ cm^{-3}, $V = -400.0$ km s^{-1}). The black dashed lines stand for the locations of the magnetic pileup boundary and the bow shock for Vignes et al. (2000) models.

($Y > 0$) seems a bit larger than at the dawnside ($Y < 0$), and the northern hemisphere ($Z > 0$) is also slightly stronger than the southern one ($Z < 0$). In addition, the crustal field can also affect the magnetic pileup result. As the strongest Martian crustal magnetic field was fixed to be located on the dayside in this work, on the X–Z plane the intense crustal field regions are mainly concentrated in the southern hemisphere. At these places, the presence of the negative values of dB_t denotes that B_t decreases and the magnetic pileup does not occur there. Although, some weaker pileups still occur outside these negative dB_t regions. In other words, the magnetic pileup is generally weak in the intense crustal field region and strong in the weak crustal field region. Besides, the decrease in magnetic field strength in panel (d) might be due to the solar wind compression and the complex topology of the Martian crustal field, as we mentioned above.

3. Results and Discussions

3.1. Results

As the magnetic pileup is expected to be related to the IMF conditions, we first investigated the magnetic pileup at Mars caused by the different IMF components as shown in Figure 2. It displays that the radial IMF component, B_X, has little effect on the magnetic pileup at Mars, while the perpendicular components, B_Y and B_Z, mainly dominate the magnetic pileup process. Similar to Figure 1, the magnetic pileup generally occurs at the dayside region for the B_Y and B_Z conditions, and the pileup intensity is generally decreasing with increasing SZA. Moreover, the effect of the crustal field also shows that the magnetic pileup is generally weak in the intense crustal field region, while it is strong in the weak crustal field region. However, in the southern hemisphere of the X–Z plane, the pileup conditions are much more complicated under the different IMF orientations. Under the northward B_Z, two large regions with the negative value of dB_t alternately take place. At

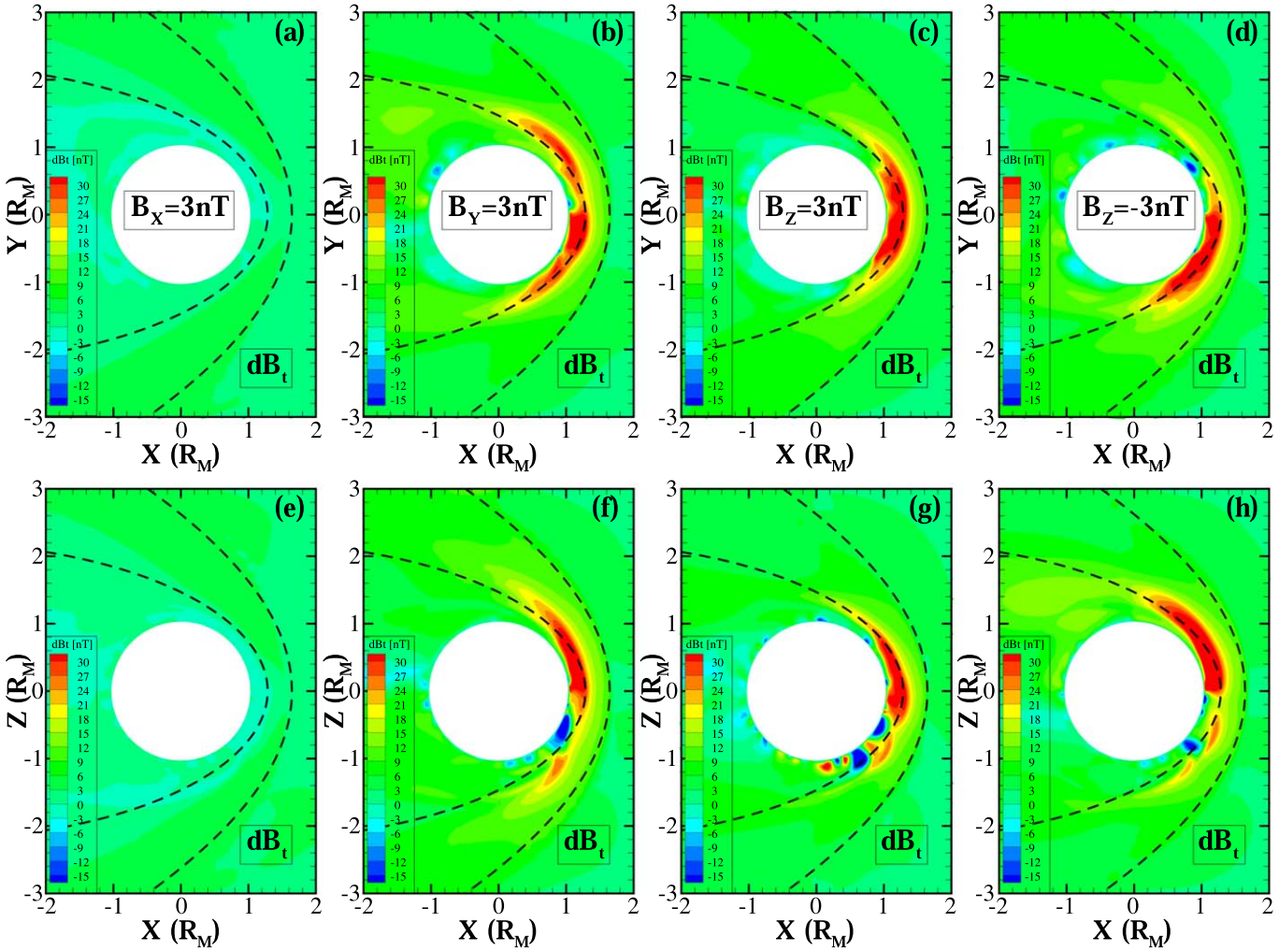

Figure 2. IMF components influence on the magnetic pileup at Mars represented by the difference in magnetic field intensity, dB_t, on the X–Y (upper panels) and X–Z (bottom panels) planes in the MSO coordinate system for $P_d = 1.06$ nPa ($n = 4.0\ \mathrm{cm}^{-3}$, $V = -400.0\ \mathrm{km\ s}^{-1}$). Panels (a)–(h) display dB_t under the steady state between the IMF conditions of zero intensity (IMF = 0) and $B_X = 3$ nT ($B_Y = B_Z = 0$ nT) (panels (a) and (e)), $B_Y = 3$ nT ($B_X = B_Z = 0$ nT) (panels (b) and (f)), $B_Z = 3$ nT ($B_X = B_Y = 0$ nT) (panels (c) and (g)), and $B_Z = -3$ nT ($B_X = B_Y = 0$ nT) (panels (d) and (h)). The black dashed lines represent the locations of the magnetic pileup boundary and the bow shock for Vignes et al. (2000) models.

the same time, there is only one apparent negative dB_t region under the southward B_Z and positive B_Y conditions. In addition, at SZA $\approx 45°$ on the southern hemisphere of the X–Z plane, the pileup ($+dB_t$) occurs under the northward B_Z, while the negative dB_t dominates at the same place under the southward B_Z. We suggest this phenomenon is related to the local magnetic reconnection conditions, which will be discussed in detail later.

Next, we studied the effect of the solar wind dynamic pressure constituted with different densities and velocities on the magnetic pileup condition at Mars, as shown in Figure 3. Panels (a) and (d) display that, under the same dynamic pressure, for a higher solar wind velocity the intensity of the magnetic pileup is stronger, and the pileup region is more extensive, which agrees with the result of Wang et al. (2021, 2022). Moreover, the increased pileup mainly occurs at the dayside region just outside the MPB of the Vignes et al. (2000) model, and it also decreases with increasing SZA. When P_d increases (panels (b), (c), (e), and (f)), the magnitude of the magnetic pileup is enhanced, while the pileup region shrinks to the Martian surface. Accordingly, the regions with the negative values of dB_t appear outside the pileup region, especially at the locations of the MPB and the bow shock. At last, the magnetic pileup displays some asymmetries due to the increasing solar wind dynamic pressure (or the velocity). At the dayside, when P_d (or velocity) increases, the pileup at the duskside hemisphere ($Y > 0$) is a bit larger than that at the dawnside ($Y < 0$). Moreover, the pileup in the southern hemisphere is generally stronger than in the northern hemisphere, which might be due to the higher altitude of the MPB caused by the intense crustal field.

As the solar wind flows around the Martian induced magnetosphere, due to the draping of the IMF, the magnetic field tends to be a quasiradial orientation at the nightside (e.g., Crider et al. 2004). Meanwhile, the solar wind can concentrate the magnetic field lines to the center of the magnetotail, where the magnetic field intensity can also be affected. Figure 3 shows that when P_d (or velocity) increases, at the center of the induced magnetotail ($Y \approx 0$) on the X–Y plane the duskside hemispheres ($Y > 0$) display the negative dB_t, while the positive dB_t regions appear at the dawnside hemisphere ($Y < 0$). On the X–Z plane at $Z \approx 0$, the northern hemispheres ($Z > 0$) show the positive dB_t, while the southern ones ($Z < 0$) display the negative dB_t. The reason for the asymmetric dB_t (or

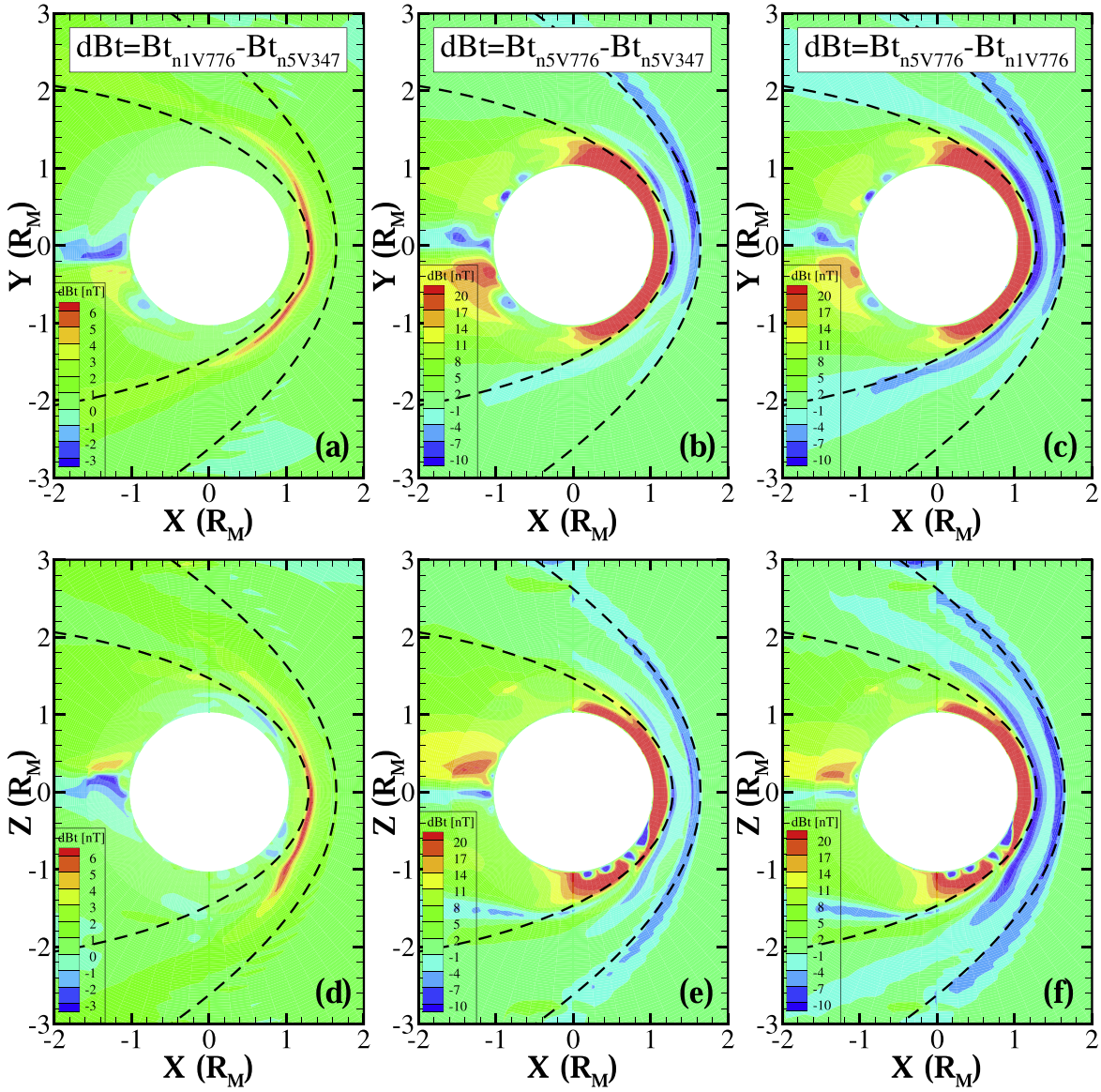

Figure 3. The solar wind dynamic pressure effect on the magnetic pileup condition at Mars represented by the difference in magnetic field intensity, dB_t, on the X–Y (upper panels) and X–Z (bottom panels) planes in the MSO coordinate system for the Parker-spiral IMF condition. Left panels (a) and (d) show dB_t under the same P_d (1 nPa) between $n = 1$ cm^{-3}, $V = -776$ km s^{-1} and $n = 5$ cm^{-3}, $V = -347$ km s^{-1}, middle panels (b) and (e) display dB_t between $P_d = 5$ nPa ($n = 5$ cm^{-3}, $V = -776$ km s^{-1}) and $P_d = 1$ nPa ($n = 5$ cm^{-3}, $V = -347$ km s^{-1}), and right panels (c) and (f) are dB_t between $P_d = 5$ nPa ($n = 5$ cm^{-3}, $V = -776$ km s^{-1}) and $P_d = 1$ nPa ($n = 1$ cm^{-3}, $V = -776$ km s^{-1}). The black dashed lines represent the locations of the magnetic pileup boundary and the bow shock for Vignes et al. (2000) models.

pileup conditions) at the center of the induced magnetotail might be related to the asymmetric current sheet at the place, which will also be discussed in detail.

3.2. Discussions

As illustrated in the introduction, the magnetic pileup is mainly associated with the deceleration of solar wind caused by both the mass loading and the ionospheric diamagnetism. However, the relation between the convection electric field and the mass loading is not intuitive. Previously, we found that a larger solar wind velocity could bring a thicker magnetic pileup region as well as a higher MPB (Wang et al. 2021). There are two reasons that may correlate the solar wind velocity to the mass loading and magnetic pileup. First, a larger solar wind velocity means a longer sweeping distance in unit time. As the density of the planetary ions is increasing with decreasing heights, the solar wind with a higher velocity should pick up more ions in unit time, leading to a stronger mass loading and a larger deceleration rate. Second, when close to the Martian ionosphere, the solar wind velocity can even drop to zero near the subsolar standoff point, where the magnetic field is significantly piled up. As a result, a higher upstream solar wind velocity corresponds to more magnetic field lines that can be convected by the solar wind and piled up near the ionopause in unit time, resulting in a thicker pileup region. As a result, a larger magnetic solar wind velocity may bring in a stronger mass loading as well as a higher diamagnetic current.

Meanwhile, the IMF can only be compressed in the direction perpendicular to the solar wind velocity, and hence only the vertical components of the IMF, B_Y and B_Z, can contribute to the pileup process. In contrast, the radial component, B_X, has no

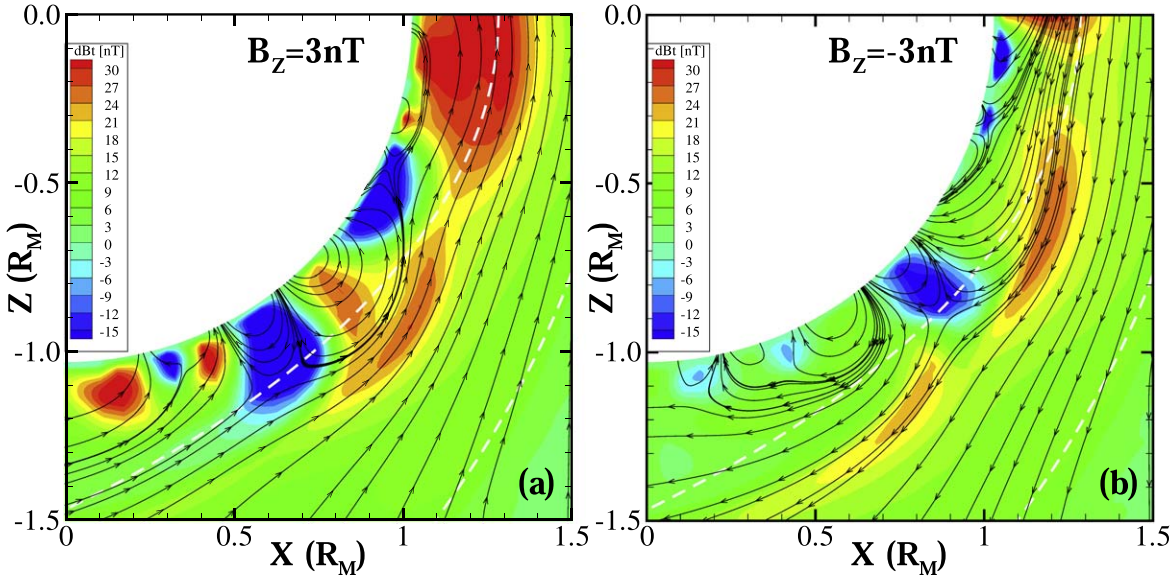

Figure 4. Relation between the magnetic field lines and the magnetic pileup condition on the southern hemisphere of *X*–*Z* plane in the MSO coordinates for $P_d = 1.06$ nPa ($n = 4.0$ cm^{-3}, $V_X = -400.0$ km s^{-1}). Panel (a) displays dB_t under the steady state between the IMF conditions of zero intensity (IMF = 0) and $B_Z = 3$ nT ($B_X = B_Y = 0$ nT) (same as panel (g) of Figure 2), and panel (b) shows the corresponding condition under $B_Z = -3$ nT ($B_X = B_Y = 0$ nT) (same as panel (h) of Figure 2). The solid black lines are the magnetic field lines, and the white dashed lines represent the locations of the magnetic pileup boundary and the bow shock for Vignes et al. (2000) models.

significant effect. This agrees with the simulation results of Venus that the induced magnetosphere is more controlled by the IMF components perpendicular to the solar wind velocity, rather than the IMF magnitude (Xu et al. 2022a). For the nonradial case (B_Y and/or B_Z condition), in the subsolar region, the IMF has the largest components perpendicular to the solar wind direction, which causes the strongest magnetic pileup. With increasing SZA angle, the perpendicular IMF components are decreased due to the pileup of the magnetic field line around the Martian ionopause, and the magnetic pileup itself is also weakened with SZA (e.g., Crider et al. 2004; Luhmann et al. 2004; Brain et al. 2005). This distribution of the perpendicular IMF components is also the reason for the dawn–dusk asymmetry of the pileup in the dayside region under the Parker-spiral IMF, as the Parker-spiral IMF contributes more perpendicular components in the duskside hemisphere. However, in this vein, the southward and northward B_Z should have the same effect on the magnetic pileup at Mars, which contradicts our results, especially on the southern hemisphere of the *Y*–*Z* plane in the MSO coordinates. We suggest that the different influences between the northward and southward B_Z on the magnetic pileup at Mars are from their different magnetic field topologies, as shown in Figure 4.

Figure 4 shows the relations between the magnetic field lines and the magnetic pileup results on the southern hemisphere of the *X*–*Z* plane in the MSO coordinates caused by the northward and southward B_Z. First, the Martian intrinsic crustal magnetic field is complex and its strongest crustal sources are mainly concentrated in the southern hemisphere in the longitude range of 150°E to 240°E and latitude range of 30°S to 85°S (e.g., Acuna et al. 1999; Connerney et al. 1999). Moreover, in this work, the subsolar location is fixed to 180°W and 0°N, which represents the strongest crustal magnetic field located on the dayside (Arkani-Hamed 2001; Ma et al. 2004). As a result, panel (a) displays that, for the northward B_Z, the crustal field and the IMF roughly point to the same direction at SZA ≈ 45° where the Martian induced magnetosphere appears as a bulged "mini-magnetopause," and the magnetic field lines are piled up upstream of it. Next, due to the "magnetic stripes" of the crustal field along the east–west direction, at the flanks of the "mini-magnetopause" (SZA ≈ 30° and 60°), the directions of the crustal field and the IMF are opposite there, which causes the X-line structure of the magnetic field indicating the occurrence of magnetic reconnection. In addition, these two regions appear the negative dB_t, while some weaker pileups still occur outside these negative dB_t regions. This implies that the magnetic reconnection can weaken the local pileup, which might be because the magnetic reconnection reduces the local magnetic field magnitude compared with the original crustal field. Under the southward IMF component in panel (b), at the same place of SZA ≈ 45°, the antiparallel directions between the crustal field and IMF result in the X-line structure and the magnetic reconnection, leading to the erosion of the crustal field, a "cusp" region, as well as the negative dB_t region. Meanwhile, the magnetic pileup mainly occurs at its flank regions (SZA ≈ 30° and 60°).

Besides the IMF direction, the flow speed can also affect the intensity of the pileup process. As the solar wind convection electric field is related to the solar wind velocity, a higher solar wind velocity can cause more picked up ions and a stronger mass loading process, and hence the value of dB_t should be linearly correlated with the velocity. It is natural that a higher solar wind velocity results in a stronger magnetic pileup process and a larger pileup region. As a result, under the same solar wind dynamic pressure, a higher solar wind velocity leads to a farther location of the MPB, especially at the subsolar region (Wang et al. 2021). Moreover, Figure 3 shows that when P_d (or velocity) increases, the dawn–dusk and north–south asymmetries of the pileup results exist at the center of the induced magnetotail, which can be explained by the asymmetric current sheet at the place as shown by Figure 5.

Figure 5 displays the parameters of dB_t, J_t, and B_X on the *Y*–*Z* plane in the MSO coordinates at $X = -1.3$ R_M under the corresponding solar wind conditions. At the Martian induced

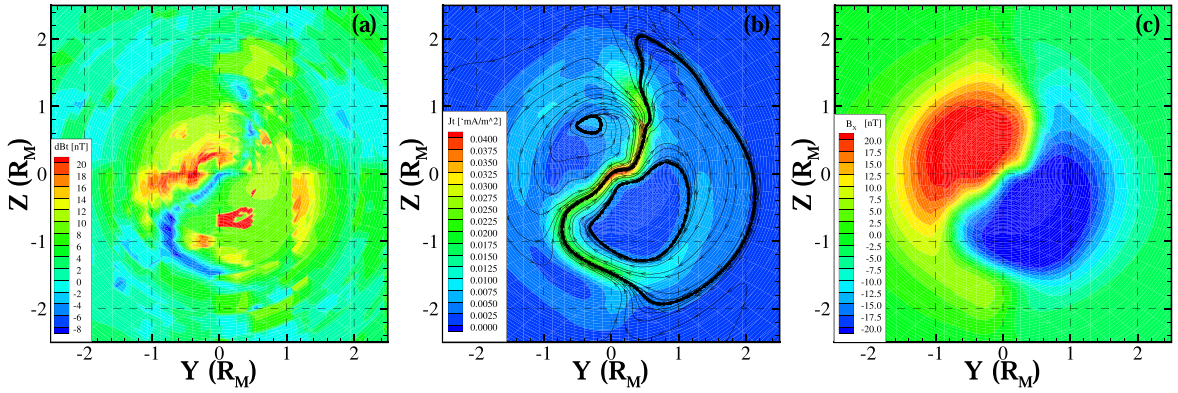

Figure 5. Topology of the difference in magnetic field intensity, the total current density, and the X component of the magnetic field on the Y–Z plane in the MSO coordinates at $X = -1.3$ R_M under the solar wind condition of $P_d = 5$ nPa ($n = 5$ cm^{-3}, $V = -776$ km s^{-1}) and the Parker-spiral IMF. Panel (a) displays the difference in magnetic field intensity, dB_t, between $P_d = 5$ nPa ($n = 5$ cm^{-3}, $V = -776$ km s^{-1}) and $P_d = 1$ nPa ($n = 5$ cm^{-3}, $V = -347$ km s^{-1}) (same as panels (b) and (e) of Figure 3). Panel (b) shows the total current density, J_t, and the black lines represent the streamlines of the Y and Z components of the current density, J_Y and J_Z. Panel (c) displays the X component of the magnetic field, B_X.

magnetotail, due to the draping of the IMF, the magnetic field tends to be a quasiradial orientation, and B_X becomes the dominant magnetic field component (e.g., Crider et al. 2004). Panel (c) shows the distribution of B_X at $X = -1.3$ R_M in the magnetotail. That is, the positive B_X is mainly located at the dawn–north section ($Y < 0$ and $Z > 0$), and a weaker striped $+B_X$ region is elongated into the southern hemisphere outside the $-B_X$ region. Conversely, the negative B_X is concentrated at the dusk-south section ($Y > 0$ and $Z < 0$), and a similar weaker striped $-B_X$ region also extends into the northern hemisphere corresponding to the $+B_X$ region. This distribution of B_X, along with the effect of B_Y (DiBraccio et al. 2018), makes the asymmetric current sheet shaped as an inverted "S," as shown in panel (b). Owing to this, the pileup condition in panel (a) shows that, when P_d increases, at the regions with the strong intensity of B_X, dB_t is positive, which means the magnetic field is piled up there. However, in the regions with the strong current density (which corresponds to the weak B_X region), the region with the negative dB_t displays a similar inverted "S" shape indicating a decreasing B_t at the place. As a result, Figure 3 shows the corresponding asymmetries of the pileup near the center of the magnetotail. It is worth mentioning that the result of the asymmetric pileup at the magnetotail is caused by an increasing P_d under the Parker-spiral IMF condition; hence this pileup result could be changed when the upstream solar wind conditions are changed.

The crustal field is another factor that could influence the magnetic pileup conditions on Mars. As mentioned above, the magnetic field pileup occurs due to the planetary ion pickup and solar wind mass loading processes. First, as the regional magnetized areas due to the Martian crust field would shield some regions from the pickup ion impact and deflect the ions into other regions, the Martian crustal field plays a protective role in the ion escape and pickup processes (e.g., Fang et al. 2010a; Li et al. 2011; Cui et al. 2018; Fan et al. 2019). Hence, the ion pickup and mass loading are generally weak at the intense crustal field region. Second, at the pileup region, the inside magnetic pressure is generally balanced with the outside thermal and dynamic pressure (e.g., Brain et al. 2010; Sánchez-Cano et al. 2020). At the intense crustal field region, the magnetic pressure is strong enough to resist the outside pressure, and hence the magnetic pileup is not obvious. However, at the weak crustal field region, the magnetic pressure provided by the crustal field is not strong enough to resist the outside pressure. Consequently, the magnetic fields will be compressed by the outside pressures, until the inner magnetic pressure can balance the outside pressure. As a result, the magnetic pileup is generally weak in the intense crustal field region and strong in the weak crustal field region. In addition, the diamagnetic current at the ionopause destructed by the magnetic anomalies might also contribute to it. Our simulation results also show that the Martian pileup is stronger when the intense crustal field is located at the nightside than at the dayside (Owing to the figure limit, we do not show them here). Next, as the magnetic reconnection can weaken the local pileup result, the variable magnetic field topologies can change the local magnetic reconnection conditions, which would also affect the magnetic pileup situations. Moreover, the anomalous crustal magnetic field and the planet's rotation all make the conditions much more complicated. In the future, the detailed effect of the crustal field on the magnetic pileup at Mars also needs to be further studied.

4. Summary and Conclusions

In this paper, using a three-dimensional multispecies MHD model, we introduced the difference in magnetic field intensity to denote the magnitude of the magnetic pileup at Mars. The effect of the IMF and the solar wind dynamic pressure constituted with different densities and velocities on the magnetic pileup were examined. Our results show that:

(1) The magnetic pileup at Mars mainly occurs at the dayside region and its magnitude is generally decreasing with increasing SZA at the pileup region. The magnetic pileup is relatively weak in the intense crustal field region and strong in the weak crustal field region.

(2) The perpendicular IMF components, B_Y and B_Z, dominate the magnetic pileup, while the radial IMF component, B_X, has little effect on it. In the intense crustal field region, the pileup condition varies with the different orientations between the IMF and crustal fields. When the IMF and crustal field primarily point in the same direction, the magnetic field is piled up and the pileup magnitude is generally strong. While the directions of the crustal field and IMF are opposite, the magnetic reconnection indicated by the X-line structure of the magnetic field can weaken the local pileup. This leads to the different pileup results on the southern hemisphere of the X–Z

plane in the MSO coordinates under the southward and northward B_Z when the intense crustal field is located on the dayside.

(3) Under the same solar wind dynamic pressure, a higher solar wind velocity results in higher intensity and a larger region of the magnetic pileup, which agrees with the previous MHD result. When P_d increases, the magnitude of the magnetic pileup is enhanced, while the pileup region shrinks. In addition, for an increasing P_d, at the center of the induced magnetotail, the asymmetric current sheet can lead to the dawn–dusk and north–south asymmetries of the pileup results.

These results need to be further examined by future observations of the Martian induced magnetosphere by multiple satellites. In this work, the intense crustal field is fixed to be located in the dayside region. Besides its anomalous distribution, the variable magnetic field topologies can change the local magnetic reconnection conditions, which would also affect the magnetic pileup situations. Moreover, the rotation of the planet makes the conditions much more complicated. In the future, the detailed effect of the crustal field on the magnetic pileup at Mars also needs to be further studied.

Acknowledgments

The work is supported by the National Natural Science Foundation of China (grant 42074195, 42030203, 41974190, 41674177, 41874208), Macau Foundation and the preresearch project on Civil Aerospace Technologies No. D020104, D020308 funded by China's National Space Administration. This research is funded by Pandeng Program of National Space Science Center, Chinese Academy of Sciences. The work is also supported by the Specialized Research Fund for State Key Laboratories, Beijing Municipal Science and Technology Commission (grant No. Z191100004319001), the Key Research Program of the Chinese Academy of Sciences, grant No. ZDBS-SSW-TLC00103, and a grant from the "Macao Young Scholars Program" (Project code: AM201905). We acknowledge the CSEM team in University of Michigan for the use of BATS-R-US code. The numerical calculations in this paper have been carried out on the super computing system in the Super computing Center of Nanjing University of Information Science & Technology. We especially acknowledge Yingjuan Ma at UCLA for the multispecies MHD model used in this work.

ORCID iDs

M. Wang https://orcid.org/0000-0002-3290-8721
J. Y. Lu https://orcid.org/0000-0001-7042-5395
Y. Wei https://orcid.org/0000-0001-7183-0229
Z. Zhou https://orcid.org/0000-0002-4463-8407
L. Chai https://orcid.org/0000-0001-8844-9176
Q. Chang https://orcid.org/0000-0003-4883-949X
H. X. Zhang https://orcid.org/0000-0002-5411-7365

References

Acuna, M. H., Connerney, J. E. P., Ness, N. F., et al. 1999, Sci, 284, 790
Arkani-Hamed, J. 2001, JGR, 106, 23197
Baumjohann, W., Blanc, M., Fedorov, A., et al. 2010, SSRv, 152, 99
Bertucci, C., Mazelle, C., Crider, D. H., et al. 2003, GeoRL, 30, 1099
Brain, D., Barabash, S., Boesswetter, A., et al. 2010, Icar, 206, 139
Brain, D. A., Halekas, J. S., Lillis, R., et al. 2005, GeoRL, 32, L18203
Brain, D. A., Mitchell, D. L., & Halekas, J. S. 2006, Icar, 182, 464
Chai, L., Wan, W., Wei, Y., et al. 2019, ApJL, 871, L27
Connerney, J. E. P., Acuna, M. H., Wasilewski, P. J., et al. 1999, Sci, 284, 794
Crider, D. H., Brain, D. A., Acuña, M. H., et al. 2004, SSRv, 111, 203
Cui, J., Yelle, R. V., Zhao, L.-L., et al. 2018, ApJL, 853, L33
DiBraccio, G. A., Luhmann, J. G., Curry, S. M., et al. 2018, GeoRL, 45, 4559
Dubinin, E., Modolo, R., Fraenz, M., et al. 2019, GeoRL, 46, 722
Fan, K., Fraenz, M., Wei, Y., et al. 2019, GeoRL, 46, 764
Fang, X., Liemohn, M. W., Nagy, A. F., et al. 2008, JGRA, 113, A02210
Fang, X., Liemohn, M. W., Nagy, A. F., et al. 2010a, Icar, 206, 130
Fang, X., Liemohn, M. W., Nagy, A. F., et al. 2010b, JGRA, 115, A04308
Fang, X., Ma, Y., Luhmann, J., et al. 2018, GeoRL, 45, 3356
Halekas, J. S., Eastwood, J. P., Brain, D. A., et al. 2009, JGRA, 114, A11204
Halekas, J. S., Ruhunusiri, S., Harada, Y., et al. 2017, JGRA, 122, 547
Harada, Y., Halekas, J. S., DiBraccio, G. A., et al. 2018, GeoRL, 45, 4550
Li, L., Zhang, Y., Feng, Y., et al. 2011, JGRA, 116, A08204
Luhmann, J. G., Ledvina, S. A., & Russell, C. T. 2004, AdSpR, 33, 1905
Luhmann, J. G., Ma, Y.-J., Brain, D. A., et al. 2015, P&SS, 117, 15
Ma, Y., Fang, X., Russell, C. T., et al. 2014a, GeoRL, 41, 6563
Ma, Y., Nagy, A. F., Sokolov, I. V., et al. 2004, JGRA, 109, A07211
Ma, Y. J., Fang, X., Nagy, A. F., et al. 2014b, JGRA, 119, 1272
Matsunaga, K., Seki, K., Brain, D. A., et al. 2017, JGRA, 122, 9723
Nagy, A. F., Winterhalter, D., Sauer, K., et al. 2004, SSRv, 111, 33
Øieroset, M., Mitchell, D. L., Phan, T. D., et al. 2004, SSRv, 111, 185
Ramstad, R., Brain, D. A., Dong, Y., et al. 2020, NatAs, 4, 979
Rong, Z. J., Stenberg, G., Wei, Y., et al. 2016, JGRA, 121, 978
Sánchez-Cano, B., Narvaez, C., Lester, M., et al. 2020, JGRA, 125, e28145
Szegö, K., Glassmeier, K.-H., Bingham, R., et al. 2000, SSRv, 94, 429
Tóth, G., van der Holst, B., Sokolov, I. V., et al. 2012, JCoPh, 231, 870
Vennerstrom, S., Olsen, N., Purucker, M., et al. 2003, GeoRL, 30, 1369
Vignes, D., Mazelle, C., Rème, H., et al. 2000, GeoRL, 27, 49
Wang, J., Lee, L. C., Xu, X., et al. 2020a, A&A, 642, A34
Wang, M., Lee, L. C., Xie, L., et al. 2021, A&A, 651, A22
Wang, M., Sui, H. Y., Lu, J. Y., et al. 2022, A&A, 664, A74
Wang, M., Xie, L., Lee, L. C., et al. 2020b, ApJ, 903, 125
Wei, Y., Fraenz, M., Dubinin, E., et al. 2012, JGRA, 117, A03208
Xu, Q., Xu, X., Zuo, P., et al. 2022a, ApJ, 931, 95
Xu, X., Lee, L. C., Xu, Q., et al. 2022b, Fundam. Res., in press